

# Spatio-temporal instability in mixed convection boundary layers

By P. MORESCO AND J. J. HEALEY

Mathematics Department, Keele University, Staffordshire ST5 5BG, UK

(Received 27 March 1999 and in revised form 10 August 1999)

In this work we analyse the stability properties of the flow over an isothermal, semi-infinite vertical plate, placed at zero incidence to an otherwise uniform stream at a different temperature. Near the leading edge the boundary layer resembles Blasius flow, but further downstream it approaches that of pure buoyancy-driven flow. A coordinate transformation that describes in a smooth way the evolution between these two limiting similarity states, where the viscous and buoyancy forces are respectively dominant, is used to calculate the basic flow. The stability of this flow has been investigated by making the parallel flow approximation, and using an accurate spectral method on the resulting stability equations. We show how the stability modes discussed by other authors can be followed continuously between the forced and free convection limits; in addition, new instability modes not previously reported in the literature have been found. A spatio-temporal stability analysis of these modes has been carried out to distinguish between absolute and convective instabilities. It seems that absolute instability can only occur when buoyancy forces are opposed to the free stream and when there is a region of reverse flow. Model profiles have been used in this latter case beyond the point of boundary layer separation to estimate the range of reverse flows that support absolute instability. Analysis of the Rayleigh equations for this problem suggests that the absolute instability has an inviscid origin.

---

## 1. Introduction

Linear stability analysis has proven successful in the description of the first stages of the transition to turbulence in a great variety of physical flows. This can be accomplished by investigating the response of the flow to planar and oblique wave perturbations of various frequencies. When a physical mechanism is present that can transfer energy from the basic flow to these perturbations, they may grow in space and/or time until they are intense enough to trigger nonlinear effects and eventually generate turbulence. The linear stability analysis consists of determining the complex wavenumbers and frequencies of the waves that the system supports, and whose imaginary parts describe the growth or decay of these waves. In most previous studies of thermal boundary layers either a purely temporal or spatial instability approach was taken. For the former, the imaginary part of the frequency is non-zero and the wavenumber is taken to be real; the asymptotic growth in time of the wave amplitude is then governed by the imaginary part of the frequency. In the spatial analysis, the frequency is real and the wavenumber is allowed to be complex; the spatial growth rate is then determined by the imaginary part of the wavenumber. The second approach is preferred in making comparisons with experiments, where the boundary layer is often perturbed with waves of fixed frequency. But the limitations

of adopting a purely spatial or temporal instability analysis were made clear with the introduction of the concepts of absolute and convective instability, first in the field of plasma physics by Twiss (1951), Landau & Lifshitz (1954, 1959), Briggs (1964) and Bers (1975); and later in hydrodynamics by Gaster (1968), Tam (1971), Huerre & Monkewitz (1990, 1985) and Brevdo (1995) among others. They concluded that the election of a temporal or spatial analysis cannot be based exclusively on physical intuition, and can only be determined after the behaviour of both the wavenumber and frequency have been studied in the complex plane, and the convective or absolute character of the instability has been determined. This classification is significant when the Galilean invariance of the flow is broken, for example because of the boundary conditions, as this determines a privileged reference frame or 'laboratory frame'. In a convectively unstable flow, the disturbance is convected away from the point of excitation, eventually decaying to zero at all points in the flow in the laboratory frame. In the case of absolute instability, the initial impulse grows in time, both upstream and downstream, eventually contaminating the entire flow. These characteristics are in turn relevant to the local–global properties of the flow as explained by Huerre & Monkewitz (1990). For a flow convectively unstable everywhere, the dynamics are determined by the characteristics of the external excitations, and the system behaves as a spatial amplifier. By contrast, the evolution of temporally growing global modes is determined by initial conditions in time, and the interaction with nonlinear effects can give rise eventually to self-sustained global modes. This classification of instabilities is being increasingly applied to fluid dynamics in the search for an explanation of the transition to turbulence. An example of the theoretical approach and the consequences for an experiment is the boundary layer over a rotating disk studied by Lingwood (1995, 1996). In general the spatial analysis is appropriate for convective instability, while a spatio–temporal analysis is required if a region of absolute instability is present.

One of the paradigmatic examples of linear stability analysis is the laminar boundary layer on a flat plate, whose similarity solution is known as Blasius flow. This velocity profile has no inflection point and so is stable to inviscid perturbations, but the addition of a small amount of viscosity leads to the existence of a finite range of convectively unstable wavenumbers and frequencies.

When a non-uniform thermal field is added to the Blasius flow, for example by keeping the plate at a constant temperature different from the surrounding fluid, the resulting buoyancy force is a new source of destabilizing energy. The interaction and relative importance of buoyancy and viscosity produce a range of states known as mixed convection, intermediate between the two limiting cases where either buoyancy forces (free convection) or the external flow (forced convection) are dominant.

The stability of the mixed convection regime has not been intensively studied in the literature, basically because of the additional numerical complexity introduced by the lack of similarity solutions for the basic flow and the coupling of the energy and momentum disturbance equations. The first stability analysis of mixed convection flow along an isothermal vertical flat plate was by Mucoglu & Cheng (1978). In that case, the temporal instability of a Blasius flow perturbed by small buoyancy effects was considered. The basic flow was obtained by a local non-similarity method and the stability equations were solved by a Runge–Kutta shooting method with Kaplan (1964) filtering. They found that for assisting external flow, i.e. when the buoyancy force and external flow are in the same direction, the flow becomes increasingly stable with increasing buoyancy force, while the opposite occurs for opposing flow.

The stability properties of the mixed convection flow near the free convection

regime were analysed by Brewster & Gebhart (1991). In that case the basic flow was obtained by perturbation expansions around the pure natural convection regime, and the stability equations were solved by numerical integration with a fourth-order predictor–corrector method. Only spatial instability was considered and it was found that the external flow reduces the critical Reynolds number but makes other unstable modes less unstable. The reverse occurs for the case of opposing flow.

To understand how the instability properties of these two limiting cases are related, and what happens in between, it is necessary to carry out an analysis of the entire mixed convection regime. As far as we know, the only stability study for the entire mixed convection regime is due to Lee, Chen & Armaly (1987). They employed a coordinate transformation to obtain in a continuous way the solution of the basic flow for the whole mixed convection regime. They analysed the stability properties by solving a quasi-parallel model but, as indicated in Brewster & Gebhart (1991), this procedure is inconsistent with the boundary layer approximation. The presence of more than one instability mode (two) was first reported in that study. One of these modes agrees with the mode obtained by Brewster & Gebhart (1991) for the free convection regime. The other one corresponds to the neutral curve for the forced convection profile described in Mucoglu & Cheng (1978). The coexistence of these two modes for different mixed convection regimes was reported, but their evolution throughout the complete mixed convection regime remained incomplete, in part because of limitations in their numerical method. We are not aware of any experimental data for this physical problem, although boundary layers over heated or cooled surfaces occur in many engineering applications.

Our interest here is partly to solve the mixed convection problem with an alternative numerical procedure and different method for obtaining the basic flow, thus providing independent confirmation of earlier findings, but mainly to build up a more complete overall picture of the stability characteristics. In particular, we are interested in the convective and absolute nature of the instabilities as this has a strong bearing on the transition to turbulence. Consequently we apply a spatio–temporal analysis and use a coordinate transformation that describes in a smooth way the evolution between the two limiting similarity states proposed by Hunt & Wilks (1981). These equations were solved using the Keller-box method as described by Keller & Cebeci (1971), which is especially suited to boundary layer equations when arbitrary non-uniform grids are present, like the ones necessary for the spectral methods that we used to solve the stability equations. We are not aware of any other work where spectral methods have been used in the stability analysis of this physical problem. This method has allowed us to extend the parameter regime studied by previous investigators, and to discover new instability modes.

By taking both wavenumbers and frequencies to be complex, i.e. by using a spatio–temporal analysis, and by considering both unstable and stable modes, we were able to locate the branch points connecting modes from different Riemann surfaces of the dispersion relation. Briggs' (1964) criterion was used to distinguish between stable and unstable modes, and in the latter case to determine their convective or absolute character. Both assisting and opposing external flow were studied and, beyond the point of separation of the boundary layer, analytical models of the basic flow were used, as the numerical approach used in the other cases ceases to be valid (the boundary layer equations become singular at separation). The inviscid limit of the absolute instability was investigated by solving the corresponding Rayleigh equation. The amount of reverse flow required for absolute instability in this problem has been determined.

The paper is structured as follows: §2 gives the equations of motion, the method for calculating the basic flow and the formulation of the stability problem and Briggs criterion. This section also describes briefly the numerical methods that have been used. In §3 the different stability modes of the modified Orr–Sommerfeld equations are presented, showing their evolution as the mixed convection regime evolves between the forced convection and the free convection limits. Dispersion curves are shown where the Briggs criterion can be applied to distinguish between convective and absolute instabilities, and in the latter case the inviscid limit was studied. Conclusions and suggestions for further work are presented in §4.

## 2. Analysis

### 2.1. Equations of fluid motion

In this work we study the stability characteristics of the boundary layer in a uniform stream over a semi-infinite vertical plate at constant temperature. Under these conditions both viscous and buoyancy forces, resulting from the thermally induced density differences, may contribute energy to the growth in time or space of any disturbance present in the flow. The relative importance of these destabilizing mechanisms varies with the distance from the edge of the plate, and this produces substantial modifications to the stability properties. Near the leading edge of the plate, the flow is dominated by the incident stream and may be described by the Blasius similarity solution. On the other hand, as the heat is diffused from the plate to the fluid, the buoyancy forces become more important, and far away from the leading edge, the flow approximates the state of free convection (Ostrach similarity solution). Only two-dimensional disturbances will be considered here, but the extension to three-dimensional disturbances is straightforward in principle.

We use the Boussinesq approximation, and so the only fluid property to vary with temperature is the density, and this dependence is assumed to be linear. Under these conditions the equations of mass, momentum and energy conservation may be expressed as

$$\frac{\partial u}{\partial x} + \frac{\partial v}{\partial y} = 0, \quad (2.1)$$

$$\frac{\partial u}{\partial t} + u \frac{\partial u}{\partial x} + v \frac{\partial u}{\partial y} = \nu \nabla^2 u \pm \beta g (T - T_0) - \frac{1}{\rho_0} \frac{\partial p}{\partial x}, \quad (2.2)$$

$$\frac{\partial v}{\partial t} + u \frac{\partial v}{\partial x} + v \frac{\partial v}{\partial y} = \nu \nabla^2 v - \frac{1}{\rho_0} \frac{\partial p}{\partial y}, \quad (2.3)$$

$$\frac{\partial T}{\partial t} + u \frac{\partial T}{\partial x} + v \frac{\partial T}{\partial y} = \kappa \nabla^2 T, \quad (2.4)$$

where  $\rho_0$  is the mean density,  $g$  is the gravitational acceleration,  $\nu$ ,  $\kappa$  and  $\beta$  are the kinematic viscosity, thermal diffusivity and coefficient of thermal expansion of the fluid respectively. The downstream coordinate is  $x$  and  $y$  is perpendicular to the plate,  $u$  and  $v$  are the corresponding components of the velocity vector,  $p$  is the pressure and  $t$  is the time. The temperature field is described by  $T$ , the plate is kept at constant temperature  $T_1$  and the fluid far from the plate has velocity  $U_0$  in the  $x$ -direction and temperature  $T_0$ . The plus and minus signs in the buoyancy term correspond to the situations where the external flow and the buoyancy force are in the same direction (assisting flow), and when they are in opposite directions (opposing flow) respectively.

The appropriate boundary conditions for equations (2.1)–(2.4) are  $u = v = 0$ ,  $T = T_1$  on  $y = 0$ , and  $u \rightarrow U_0$ ,  $T \rightarrow T_0$  as  $y \rightarrow \infty$ .

## 2.2. The basic flow

Equations (2.1)–(2.4) can be re-written using a stream function formalism, which reduces the number of equations and eliminates the pressure. Furthermore, applying the boundary layer approximations for steady flow the following set of equations is obtained:

$$\frac{\partial \psi}{\partial y} \frac{\partial^2 \psi}{\partial y \partial x} - \frac{\partial \psi}{\partial x} \frac{\partial^2 \psi}{\partial y^2} = \nu \frac{\partial^3 \psi}{\partial y^3} \pm \beta g(T - T_0), \quad (2.5)$$

$$\frac{\partial \psi}{\partial y} \frac{\partial T}{\partial x} - \frac{\partial \psi}{\partial x} \frac{\partial T}{\partial y} = \kappa \frac{\partial^2 T}{\partial y^2}, \quad (2.6)$$

where  $\psi$  is the stream function for the basic flow defined by

$$u = \frac{\partial \psi}{\partial y}, \quad v = -\frac{\partial \psi}{\partial x}. \quad (2.7)$$

The mixed convection flow presents the additional difficulty that it lacks similarity solutions. In most of the previous works, either non-similarity methods or asymptotic expansions were used, but in the former it is difficult to estimate the magnitude of the errors, and the latter are useful only near to the similarity regimes. To describe in a continuous form the evolution between the two asymptotic regimes, where the viscous and buoyancy forces are respectively dominant, we adopted the transformation for the stream function and temperature distribution proposed by Hunt & Wilks (1981).

Under this transformation the following characteristic velocity,  $U_c$ , temperature,  $T_c$ , and length,  $\delta$ , are defined:

$$U_c = U_0(1 + \xi)^{1/2}, \quad T_c = T_1 - T_0, \quad \delta = \left( \frac{2\nu x}{U_0} \right)^{1/2} \frac{1}{(1 + \xi)^{1/4}}. \quad (2.8)$$

The non-dimensional buoyancy parameter  $\xi$  measures the relative importance of the viscous–inertia and buoyancy forces and is defined as

$$\xi = \frac{|Gr_x|}{Re_x^2}, \quad Gr_x = \frac{g\beta(T_1 - T_0)x^3}{\nu^2}, \quad Re_x = \frac{U_0 x}{\nu}, \quad (2.9)$$

where  $Gr_x$  and  $Re_x$  are the local Grashof and Reynolds numbers based on the distance from the leading edge. For  $\xi = 0$ , the flow is equivalent to a Blasius profile, as  $\xi \rightarrow \infty$  it evolves towards a free convection regime and when  $\xi = O(1)$  the buoyancy and viscosity–inertia terms are comparable. The non-dimensional stream function,  $f$ , temperature field,  $\theta$ , and coordinate normal to the plate,  $\eta$ , are defined using the quantities introduced in (2.8) as

$$f(\xi, \eta) = \frac{\psi}{U_c \delta}, \quad (2.10)$$

$$\theta(\xi, \eta) = \frac{T - T_0}{T_c}, \quad (2.11)$$

$$\eta = \frac{y}{\delta}. \quad (2.12)$$

Using these transformations, (2.5)–(2.6) can be written as

$$\frac{\partial^3 f}{\partial \eta^3} + \frac{(4 + 6\xi)}{4(1 + \xi)} f \frac{\partial^2 f}{\partial \eta^2} - \frac{\xi}{\xi + 1} \left( \frac{\partial f}{\partial \eta} \right)^2 \pm \frac{2\xi\theta}{1 + \xi} = 2\xi \left\{ \frac{\partial^2 f}{\partial \xi \partial \eta} \frac{\partial f}{\partial \eta} - \frac{\partial^2 f}{\partial \eta^2} \frac{\partial f}{\partial \xi} \right\}, \quad (2.13)$$

$$\frac{1}{Pr} \frac{\partial^2 \theta}{\partial \eta^2} + \frac{(4 + 6\xi)}{4(1 + \xi)} f \frac{\partial \theta}{\partial \eta} = 2\xi \left\{ \frac{\partial f}{\partial \eta} \frac{\partial \theta}{\partial \xi} - \frac{\partial f}{\partial \xi} \frac{\partial \theta}{\partial \eta} \right\}, \quad (2.14)$$

where  $Pr$  is the Prandtl number, taken to be constant and equal to 0.733, which corresponds to air under atmospheric conditions. The corresponding boundary conditions are:  $f = \partial f / \partial \eta = 0$ ,  $\theta = 1$  on  $\eta = 0$ ; and  $\partial f / \partial \eta \rightarrow (1 + \xi)^{-1/2}$ ,  $\theta \rightarrow 0$  as  $\eta \rightarrow \infty$ . The non-slip boundary condition on the plate breaks the Galilean invariance, singling out a particular ‘laboratory frame’. This set of equations is valid throughout the mixed convection regime, as  $\xi$  varies from  $\xi = 0$  (forced convection) to  $\xi \rightarrow \infty$  (free convection).

### 2.3. Linear perturbation analysis

The motion is now decomposed into a mean flow which is supposed steady (basic flow) and a superimposed disturbance (primed variables):

$$\tilde{u}(x, y, t) = u(x, y) + u'(x, y, t), \quad (2.15)$$

$$\tilde{v}(x, y, t) = v(x, y) + v'(x, y, t), \quad (2.16)$$

$$\tilde{p}(x, y, t) = p(x, y) + p'(x, y, t), \quad (2.17)$$

$$\tilde{T}(x, y, t) = T(x, y) + T'(x, y, t). \quad (2.18)$$

Substituting these equations in (2.1)–(2.4) the terms containing only basic flow quantities can be eliminated, as they satisfy (2.5)–(2.6). For small amplitudes we neglect the nonlinear combinations of perturbation quantities, which leads to the linearized disturbance equations:

$$\frac{\partial u'}{\partial x} + \frac{\partial v'}{\partial x} = 0, \quad (2.19)$$

$$u' \frac{\partial u}{\partial x} + v' \frac{\partial u}{\partial y} + \frac{\partial u'}{\partial t} + u \frac{\partial u'}{\partial x} + v \frac{\partial u'}{\partial y} = \nu \nabla^2 u' \pm g\beta T' - \frac{1}{\rho_0} \frac{\partial p'}{\partial x}, \quad (2.20)$$

$$u' \frac{\partial v}{\partial x} + v' \frac{\partial v}{\partial y} + \frac{\partial v'}{\partial t} + u \frac{\partial v'}{\partial x} + v \frac{\partial v'}{\partial y} = \nu \nabla^2 v' - \frac{1}{\rho_0} \frac{\partial p'}{\partial y}, \quad (2.21)$$

$$u' \frac{\partial T}{\partial x} + v' \frac{\partial T}{\partial y} + \frac{\partial T'}{\partial t} + u \frac{\partial T'}{\partial x} + v \frac{\partial T'}{\partial y} = \kappa \nabla^2 T'. \quad (2.22)$$

In order to exploit a normal mode structure for the disturbances, it is necessary to make a parallel flow approximation, where the wavenumber, frequency and basic flow quantities are taken to be independent of the  $x$ -coordinate. This is supposed to be justified provided that the waves of interest have a length that can be considered small compared to the distances over which the boundary layer is growing. For a more detailed description of the conditions in which the parallel approximation is valid see Brevdo & Bridges (1997).

Thus, we take

$$u = u(y), \quad v \equiv 0, \quad T = T(y), \quad (2.23)$$

and a solution of the form

$$\psi' = \tilde{\phi}(y)e^{i(\alpha x - \omega t)}, \quad T' = \tilde{\zeta}(y)e^{i(\alpha x - \omega t)}, \quad (2.24)$$

where  $\psi'$  is the stream function of the perturbation and  $T'$  its temperature distribution function.

Using the same characteristic quantities defined in (2.8) for the basic flow, the amplitude functions of the disturbance stream function and temperature, the wavenumber  $\alpha$  and frequency  $\omega$  are non-dimensionalized as

$$\phi = \frac{\tilde{\phi}}{\delta U_c}, \quad s = \frac{\tilde{\zeta}}{T_c}, \quad (2.25)$$

$$\omega = \tilde{\omega} \frac{\delta}{U_c}, \quad \alpha = \tilde{\alpha} \delta, \quad (2.26)$$

where the tilde denotes dimensional quantities. Substituting (2.23) and (2.24) into (2.19)–(2.22) the following non-dimensional stability equations are obtained:

$$(\phi'' - \alpha^2 \phi) \left( \bar{u} - \frac{\omega}{\alpha} \right) - \phi \bar{u}'' = \frac{1}{i\alpha Re_\delta} \left( \phi^{iv} - 2\alpha^2 \phi'' + \alpha^4 \phi \pm \frac{2\xi}{\xi + 1} s' \right), \quad (2.27)$$

$$s \left( \bar{u} - \frac{\omega}{\alpha} \right) - \phi \bar{T}' = \frac{1}{i\alpha Re_\delta Pr} (s'' - \alpha^2 s), \quad (2.28)$$

where the primes denote derivatives with respect to  $\eta$ , which is now just a non-dimensional  $y$ -variable due to the parallel flow approximations. The barred quantities correspond to the non-dimensionalized basic flow and are defined using the solutions to (2.13)–(2.14) as

$$\bar{u} = \frac{\partial f}{\partial \eta}, \quad \bar{u}'' = \frac{\partial^3 f}{\partial \eta^3}, \quad \bar{T}' = \frac{\partial \theta}{\partial \eta}, \quad (2.29)$$

and the Reynolds number is defined as

$$Re_\delta = \frac{U_c \delta}{\nu}. \quad (2.30)$$

The corresponding homogeneous boundary conditions for equations (2.27)–(2.28) are

$$\phi(0) = \phi'(0) = s(0) = \phi(\infty) = \phi'(\infty) = s(\infty) = 0, \quad (2.31)$$

satisfying non-slip and zero normal velocity at the wall, decaying disturbances in the free stream and the prescribed temperature boundary conditions.

In this work we carry out a spatio-temporal stability analysis and consequently both the wavenumber  $\alpha$  and the frequency  $\omega$  will be taken to be complex numbers. Solutions of these two coupled ordinary differential equations that satisfy the homogeneous boundary conditions only exist for certain combinations of the complex parameters  $\alpha$  and  $\omega$ . We will denote with subscripts  $r$  and  $i$  the real and imaginary parts of the variables respectively. Given two of  $\alpha_r, \alpha_i, \omega_r, \omega_i$ , the other pair appears as eigenvalues of these equations, satisfying a dispersion relation of the form

$$D(\omega, \alpha) = 0. \quad (2.32)$$

The complexity of the dispersion relation for this problem makes it necessary to obtain its solution using numerical methods that will be described in §2.6.

*2.4. Classification of instabilities*

As described in §1, the stability properties of the perturbations were determined using a spatio-temporal analysis and the Briggs criterion. This is based on the study of the long time behaviour of an impulsive response of an infinite system to a localized excitation that is zero for  $t < 0$ . This initial value problem corresponds to the inhomogeneous equivalent of (2.27)–(2.28) and its solution can be expressed in the form of a Green function in spectral space  $G(\alpha, \omega)$ , which can be converted to the physical space through inverse Laplace and Fourier transforms of the form

$$G(x, t) = \frac{1}{(2\pi)} \int_A \int_F \frac{e^{i(\alpha x - \omega t)}}{D(\alpha, \omega)} d\omega d\alpha, \quad (2.33)$$

where the denominator in the integrand corresponds to the dispersion relation introduced in (2.32). The Bromwich contour  $F$  in the  $\omega$ -plane is a horizontal line lying above all the singularities to satisfy causality, and the integration path  $A$  lies inside the analyticity band around the real  $\alpha$ -axis. The Briggs criterion makes use of the properties of the dispersion relation, causality arguments and (2.33) to determine the absolute/convective character of the instability.

We will call a path in the  $\alpha$ -plane generated by the dispersion relation and a prescribed path in the  $\omega$ -plane a spatial branch, and a path in the  $\omega$ -plane generated by the dispersion relation and a prescribed path in the  $\alpha$ -plane a temporal branch. Causality arguments establish that for  $\omega_i$  positive and large enough all the spatial branches should lie either above or below the real axis in the  $\alpha$ -plane, without crossing the real  $\alpha$ -axis. This ensures that the flow is undisturbed far from the source. In this situation, a branch in the upper half-plane ( $\alpha_i$  positive) corresponds to a perturbation propagating downstream, and one in the lower half-plane to a perturbation propagating upstream. If when  $\omega_i$  is lowered towards zero one of the branches crosses the real  $\alpha$ -axis then it is unstable, otherwise it is stable. The Briggs criterion states that if there exists a common branch point with  $\omega_i > 0$  between two or more spatial branches, so that at least two of them lie in different  $\alpha$  half-planes for  $\omega_i$  sufficiently large, then the flow is absolutely unstable. This type of branch point is called a pinch point.

The appearance of absolute instabilities in buoyancy-induced boundary layer flows seems to be restricted to the existence of flow reversal, as found by Krizhevsky, Cohen & Tanny (1996) for the free convection flow over an isothermal vertical flat plate, immersed in a linear ambient thermal stratification. They showed that for absolute instability the value of the critical Reynolds number grows rapidly when the intensity of the reverse flow is reduced. Eventually, when no reverse flow is present there is no transition to absolute instability. This is in agreement with all the previous analyses of wall-bounded flows. In the absence of a plate, e.g. in a wake, absolute instability can occur without reverse flow. Wake stability has been studied by Betchov & Criminale (1966) using analytical models of the wake flow behind a flat plate, and more recently by Woodley & Peake (1997) who investigated the global linear stability of the same problem but using a basic state obtained by integration of the boundary layer equations.

In this work we analyse, in the case of opposing flow, how the increase of the buoyancy force, and the eventual appearance of reverse flow, gives rise to absolute instability in the mixed convection boundary layer. We relate the modes in the dispersion relation responsible for this transition to the modes present when there is only convective instability.



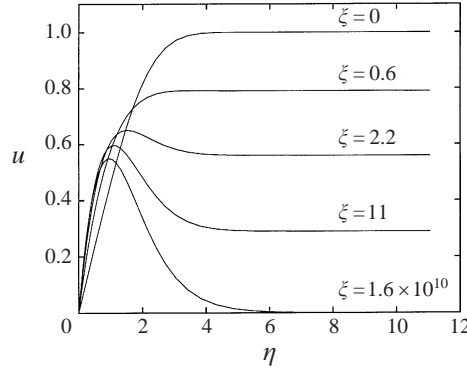


FIGURE 1. Velocity profiles of the basic flow for assisting external flow. The profile with  $\xi = 0$  corresponds to the forced convection regime, and the one for  $\xi = 1.6 \times 10^{10}$  approximates the free convection regime.

### 2.5. Inviscid limit

As some terms neglected in the parallel approximation are of the same order as terms in the Orr–Sommerfeld equations, these equations are not a consistent approximation to the full equations of motion. However a parallel–inviscid analysis is consistent since then all inverse powers of  $Re_\delta$  are neglected.

In the limit of  $Re_\delta \rightarrow \infty$ , and as we are considering  $Pr$  to be constant, (2.27)–(2.28) take the form

$$\left( \frac{\alpha \bar{u}''}{\alpha \bar{u} - \omega} + \alpha^2 \right) \phi - \phi'' = 0, \quad (2.34)$$

$$s(\alpha \bar{u} - \omega) - \phi \alpha \bar{T}' = 0, \quad (2.35)$$

resulting in the partial decoupling of the velocity and temperature disturbance equations. Equation (2.34) has the same form as the Rayleigh equation for the Blasius flow. As the boundary conditions for  $s$  are the same as those for  $\phi$ , it is sufficient to solve for  $\alpha$  and  $\omega$  in (2.34), so that  $\phi$  is bounded as  $\eta \rightarrow \infty$ , and then to calculate  $s$  from (2.35) if required. The only effect of the temperature field in the inviscid stability problem is therefore through its modification of the basic velocity profile. The inviscid problem will be studied because it allows us to determine whether the fundamental instability mechanisms are viscous or inviscid in origin, and to help us to understand the behaviour of the viscous problem at Reynolds numbers that are too high for the numerical methods.

### 2.6. Numerical methods

The basic flow equations (2.13) and (2.14) were solved using the Keller-box method described in Keller & Cebeci (1971), which is well suited for parabolic partial differential equations. In this method the partial differential equations are written as a first-order system and centred difference quotients and averages at the midpoints of a rectangular net in  $\eta$  and  $\xi$  are used to transform it into finite difference equations. In the  $\eta$ -direction a grid of 360 points in the interval  $[0, 12]$  was used, including the collocation points later employed in the pseudospectral solution of the stability problem. Extrapolation was used for the collocation points lying outside that range. A variable integration step was used in  $\xi$ , corresponding to 0.01% of the  $\xi$  value in the previous step. The resulting highly implicit and nonlinear equations were solved using the Powell Hybrid Method (from the MINPACK Fortran library). In figure 1

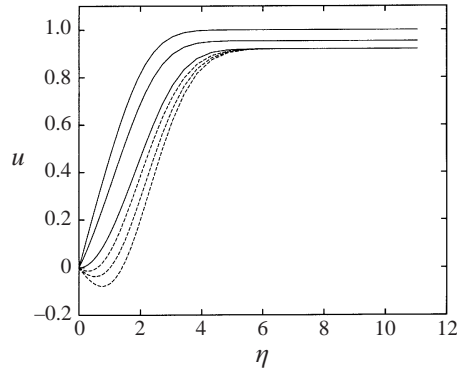


FIGURE 2. Velocity profiles of the basic flow for opposing external flow. The continuous lines correspond to solutions of equations (2.13)–(2.14) obtained with the Keller-box method. The dashed lines correspond to solutions of equation (2.36) used to model the flow after the separation of the boundary layer. For increasing reverse flow the parameters are  $(a = -0.25, b = 0.92, c = 0.09, d = 0.09)$ ,  $(a = -0.25, b = 0.92, c = 0.13, d = 0.13)$  and  $(a = -0.25, b = 0.92, c = 0.17, d = 0.18)$ .

are plotted some of the velocity profiles for assisting flow at different values of  $\zeta$  obtained by solving (2.13)–(2.14) in this way.

This numerical method and equations are based on the boundary layer approximation, and so cannot be used beyond a separation point. In the case of opposing flow, separation will always occur sufficiently far from the leading edge. The extension beyond this point is obtained through model profiles of the form

$$\bar{u}(\eta) = -e^{a\eta^2}(b + c\eta + d\eta^2) + b, \quad (2.36)$$

where the parameters  $a$ ,  $b$ ,  $c$  and  $d$  were chosen to satisfy the boundary conditions and match the profile obtained numerically at the point of separation. In figure 2 some basic velocity solutions for opposing flow are presented. The continuous lines correspond to solutions of equations (2.13)–(2.14) before separation, while the dashed lines are described by (2.36).

Spectral methods provide an efficient means of solving stability equations because of their minimal phase errors (see Canuto *et al.* 1988), usually offering more accurate results than finite-difference methods, even using coarser grids. In this work, linear combinations of Chebyshev polynomials were used as they are more suitable for asymmetric boundary conditions than the Fourier expansions, and the resulting matrices were solved with a QR algorithm. The two stability equations were integrated in  $\eta$  in the interval  $[0, 256]$  using 45 collocation points (giving 90 eigenvalues). We have used a spectral stability code kindly provided by Th. Herbert and described in Herbert (1990). It can be used to obtain discrete approximations to both the discrete and continuous spectra and to distinguish between them.

The inviscid equation (2.34) was solved using a method developed by Healey (1998). To avoid the singularity at the critical point,  $\eta_c$  (where  $\alpha\bar{u}(\eta_c) = \omega$ ), a contour of integration in the complex  $\eta$ -plane was chosen so that it passes below the singularity when  $\bar{u}'(\eta_c) > 0$  and above it when  $\bar{u}'(\eta_c) < 0$ , when  $\eta_c$  is real. A shooting method with Runge–Kutta integration was then used to solve the equations for the values of  $\alpha$  and  $\omega$  for which the solution satisfies the boundary conditions.

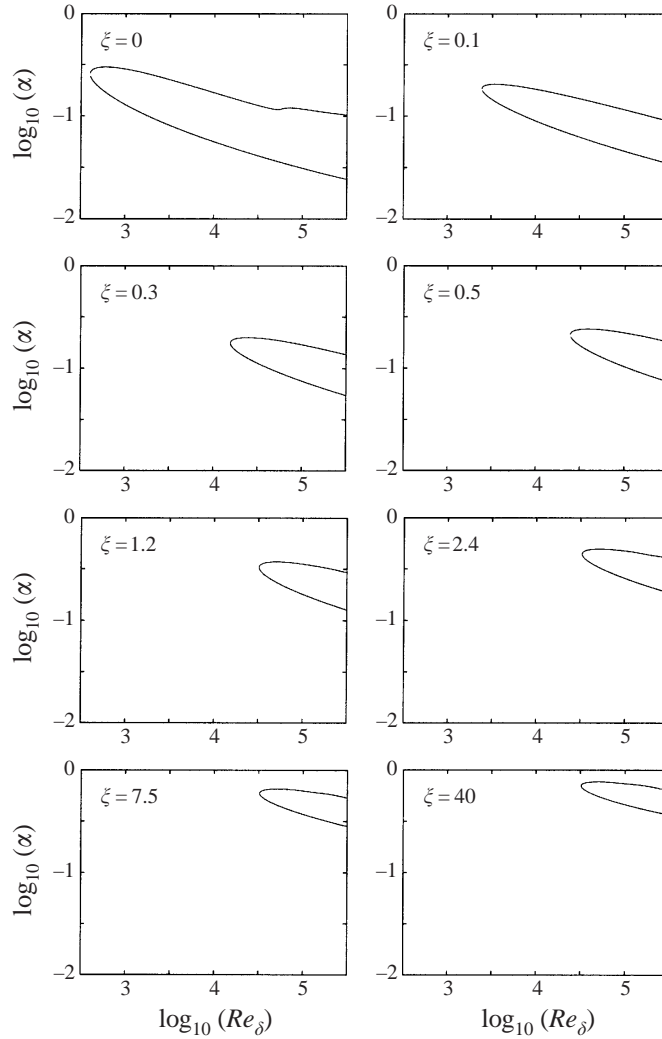


FIGURE 3. Evolution of the neutral curve of the forced convection stability mode as  $\zeta$  is increased, i.e. as buoyancy forces become more important.

### 3. Results and discussion

In figures 3–5 we present the neutral stability curves (corresponding to  $\omega_i = 0$  and  $\alpha_i = 0$ ) for assisting external flow at different values of the buoyancy parameter  $\zeta$ . We indicate the values of the phase velocity  $c$  and group velocity  $v_g$  of these modes, relative to the speed of the external flow, for certain values of  $\zeta$  near the critical Reynolds number. Figure 3 corresponds to the mode that at  $\zeta = 0$  matches that of Blasius flow ( $c = 0.39$ ,  $v_g = 0.42$ ). These results are coincident for  $\zeta \approx 0$  with those of Mucoglu & Cheng (1978) corresponding to a viscous–inertial instability where the buoyancy force is weak. Near the forced convection regime the buoyancy force has a stabilizing effect for this mode, but for  $\zeta$  greater than 1, i.e. when the buoyancy forces become dominant, they have a modest destabilizing influence. The kink on the upper branch in figure 3 when  $\zeta = 0$  marks the position of a change in disturbance

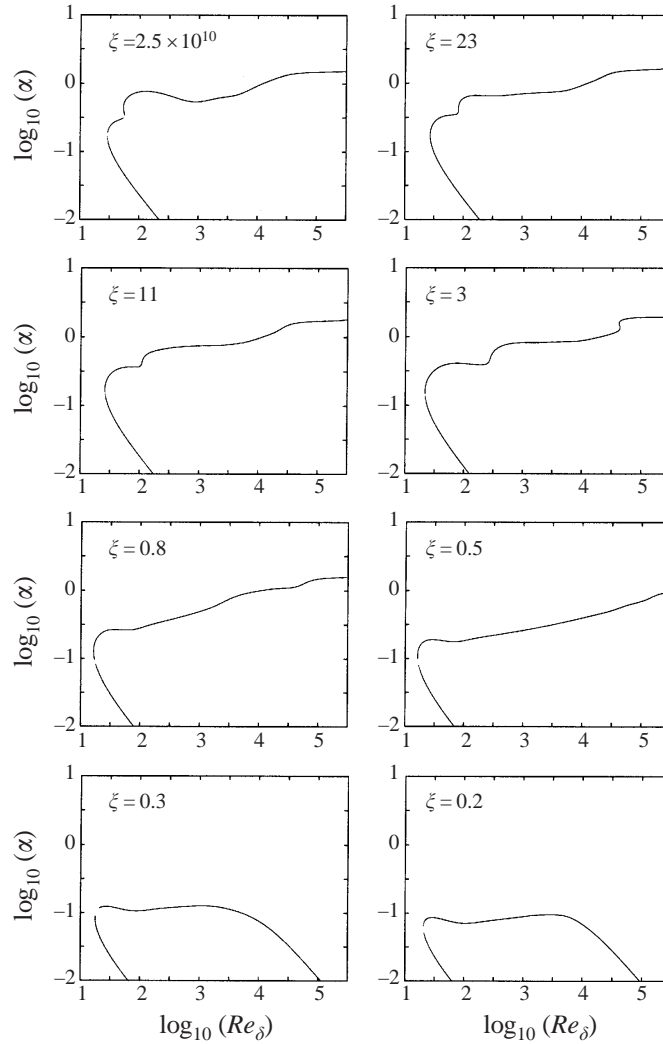


FIGURE 4. Evolution of the neutral curve of the free convection stability mode as  $\xi$  is decreased, i.e. as the external stream becomes more important.

structure, as was first shown by Healey (1995); we will use this property later in the analysis of the opposing flow case.

Figure 4 presents the evolution of the stability mode that asymptotes to the free convection solution as  $\xi \rightarrow \infty$ . As reported in Hieber & Gebhart (1971) this mode is the result of the coupling of the two instability equations (2.27)–(2.28), and its neutral curve has two critical Reynolds numbers at  $Re_\delta = 29$  and  $Re_\delta = 54$  ( $c = 0.50$ ,  $v_g = 0.32$  and  $c = 0.32$ ,  $v_g = 0.22$  respectively) at  $\xi = 2.5 \times 10^{10}$ . Although other instability modes coexist with this one over a wide range of values of  $\xi$ , this mode has the lowest values of critical  $Re_\delta$  and so may be the most relevant in the first stages of transition to turbulence, but this would need to be confirmed by a detailed analysis of the growth rates. However, as  $\xi \rightarrow 0$  the wavenumbers of this mode get smaller and smaller and presumably it becomes more affected by the non-parallel effects that have been neglected in these calculations. The presence of two critical  $Re_\delta$  at very

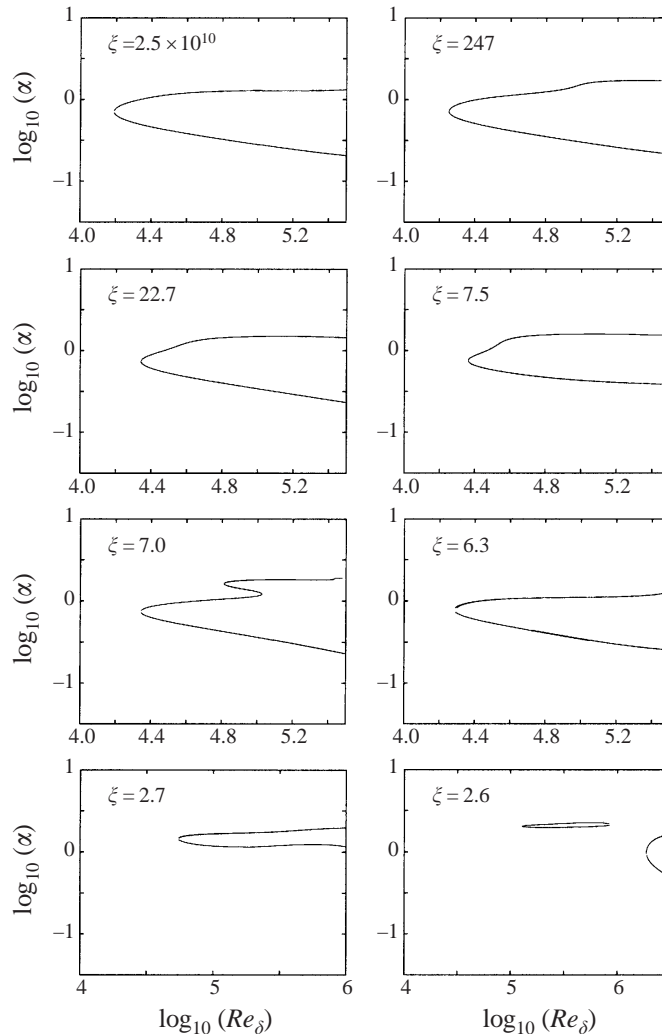


FIGURE 5. Evolution of the neutral curve of a stability mode not previously reported in the literature as  $\xi$  is decreased.

high  $\xi$  suggests the possibility of more than one stability mode becoming unstable at the same time, and then nonlinear interactions between them could lead to chaotic behaviour at low  $Re_\delta$  (this will be investigated in a future work).

Another unstable mode is shown in figure 5, that appears not to have been previously reported in the literature, but the range of  $Re_\delta$  where this mode is unstable is much higher than that for other modes ( $c = 0.26$ ,  $v_g = 0.23$ ). Small variations in  $\xi$  seem to have a significant effect on the neutral curve of this mode, especially for  $\xi \approx 7$  and  $\xi \approx 2.6$ . A further unstable mode was found for small  $\xi$  at even higher  $Re_\delta$ , suggesting that there are several unstable modes in addition to the two reported by Lee *et al.* (1987). Nevertheless all these modes and the possible wave interactions between them, have to be taken into account for a complete picture and correct classification of the mixed convection instabilities.

In the framework of a spatio-temporal analysis, we want to determine if the

presence of buoyancy forces can give rise to the appearance of absolute instability, in contrast to the Blasius flow which is known to be convectively unstable. It was found that all these modes move entirely into the upper half of the  $\alpha$ -plane as  $\omega_i$  is increased above the value defining the Bromwich contour, indicating that they correspond to perturbations propagating in the downstream direction. As pointed out by Briggs (1964), the existence of modes moving in opposite directions is a necessary condition for the existence of absolute instability, but in the case of assisting flow we could not find any mode propagating in the upstream direction. There are various branch points between these modes but they all correspond to convective instability, so it can be concluded that a spatial stability analysis is adequate for the entire mixed convection regime with assisting external flow.

In the case of opposing flow, we restrict our analysis to the regimes before and slightly after separation, because beyond this point we have to rely on the approximation to the basic flow given by (2.36). The coordinate transformation introduced in §2.2 allowed us to follow continuously the evolution of the modes presented for the case of assisting flow in the proximity of  $\zeta \approx 0$  into the case of opposing flow. We focus our attention here only on the evolution of the mode originating in the Blasius flow because the other modes only become unstable at very high Reynolds numbers (figure 5) or correspond to perturbations with very long wavelength (figure 4).

For the viscous mode described in figure 3 it can be seen in figure 6 that increasing the buoyancy force affects principally the upper branch of the neutral curve. Similar behaviour was found by Mucoglu & Cheng (1978) but no explanation was given. Qualitatively similar behaviour was found by Healey (1998) for isothermal Falkner–Skan boundary layers with negative pressure gradient. Healey found that in the absence of an inflection point in the mean profile, the kink in the upper branch marks the transition between two different asymptotic scalings of the neutral curve. To the left of the kink, and throughout the lower branch, the critical layer lies inside the viscous boundary layer, leading to a triple-deck asymptotic disturbance structure. To the right of the kink in the neutral curve, the critical layer lies outside the viscous layer giving a five-deck asymptotic structure. In the presence of an inflection point the kink marks the transition between viscous and inviscid behaviour. This can be seen from the independence of the neutral curve with respect to  $Re_\delta$ , to the right of the kink. The inclusion of thermal effects in this work does not seem to affect the basic picture described by Healey (1998). In figure 6 it can also be seen that as  $\zeta$  is increased the kink in the upper branch moves towards lower values of  $Re_\delta$  and at the point of separation ( $\zeta = 0.182$ ) the whole upper branch represents inviscid behaviour. The two plots at the bottom of figure 6 correspond to the neutral curve after separation, using the model profile described by (2.36). These two plots show very similar behaviour to that before separation and suggest that the model (2.36) is a suitable extension of (2.13)–(2.14) beyond separation. While in Blasius flow the kink is at such a high value of the Reynolds number that the change in disturbance structure associated with it is irrelevant in experimental situations, here its effects appear to be present at values of  $Re_\delta$  accessible to experiment. A similar situation is described in Healey (1998) for the Falkner–Skan problem, but it was found there that the growth of inviscid waves is small compared with that of viscous waves in typical experimental situations. However we will show below that, after the appearance of reverse flow in the mixed convection regime with opposing flow, the inviscid instability acquires an absolute character and so may be expected to be dominant over the viscous–inertial mechanism, which remains convective. Although we are not aware of experimental results concerning this physical problem, a review of the general case of separated

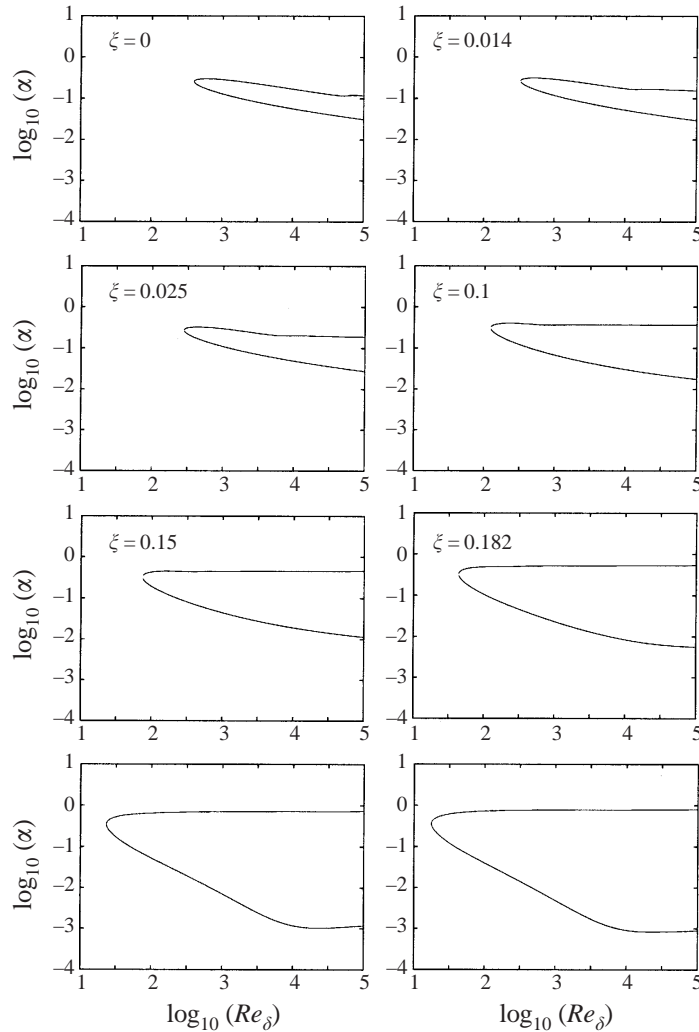


FIGURE 6. Neutral curve of the forced convection mode for opposing flow as the buoyancy force is increased. When the value of  $\xi$  is indicated the figures were obtained solving equations (2.13)–(2.14). The point  $\xi = 0.182$  corresponds to the separation of the boundary layer. The two pictures at the bottom correspond to solutions of (2.36) with parameters ( $a = -0.25$ ,  $b = 0.92$ ,  $c = 0.16$ ,  $d = 0.16$ ) on the left and ( $a = -0.25$ ,  $b = 0.92$ ,  $c = 0.23$ ,  $d = 0.22$ ) on the right.

flows, comparing both analytical and experimental results, can be found in Dovgal, Kozlov & Michalke (1994).

All the instabilities encountered for the opposing flow regime up to the point of separation were found to be convective in character but after the appearance of reverse flow the situation is different. Measuring the amount of reverse flow by the magnitude of the minimum in the velocity profile normalized by the free-stream velocity ( $\bar{u}_m$ ), we found that for values of  $\bar{u}_m$  higher than 0.152 there are two modes that produce a pinch point that satisfies the Briggs criterion for absolute instability. In figure 7 are shown two spatial branches at different values of  $\omega_i$  at  $Re_\delta = 4200$ . In figure 7(a) the branches are in different  $\alpha$ -half-planes, so the one with positive  $\alpha_i$  corresponds to a wave propagating downstream and, as it crosses the real axis when  $\omega_i$  is reduced, as in

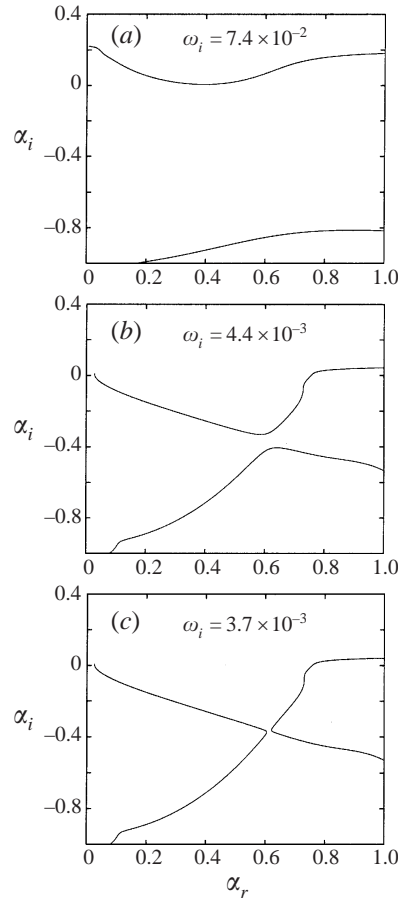


FIGURE 7. Two spatial branches that for  $\omega_i > 2.0 \times 10^{-2}$  are contained in different  $\alpha$ -half-planes, and that when  $\omega_i$  is decreased lead to a pinch point. The amount of reverse flow corresponds to  $\bar{u}_m = 0.152$  ( $a = -0.25$ ,  $b = 0.92$ ,  $c = 0.23$ ,  $d = 0.22$ ) and  $Re_\delta = 4200$ .

figure 7(b), it becomes unstable. The branch in the negative  $\alpha_i$ -half-plane corresponds to a perturbation moving upstream and is stable because it remains in the same  $\alpha$ -half-plane when  $\omega_i$  is decreased. This mode becomes increasingly damped when the amount of reverse flow is reduced and rapidly moves towards large values of  $|\alpha_i|$ . In figure 7(b,c) it can be seen how both modes approach each other and a pinch point occurs between them with subsequent branch interchange. As the value of  $\bar{u}_m$  (the amount of reverse flow) is decreased, the value of  $Re_\delta = Re_\delta^A$  at which the pinch point occurs for  $\omega_i > 0$  increases.

In a similar way, for a fixed value of  $Re_\delta = 4200$ , both spatial branches move far away from each other as the amount of reverse flow is reduced, as shown in figure 8, and the value of  $Re_\delta^A$  appears to increase towards infinity, suggesting that the inviscid theory would be helpful in this limit. To obtain a better approximation of the minimum amount of reverse flow required for the absolute instability to develop, i.e. for the pinch point to occur at positive  $\omega_i$ , and to verify that it is not an artifact of the parallel flow approximation, the inviscid stability of this flow has been studied. Figure 9 shows the behaviour of the inviscid spatial branches for  $\bar{u}_m = 0.145$ , where the pinch point is found to occur at  $\omega_i = 1.0 \times 10^{-5}$ , i.e. for  $\omega_i \approx 0$ . For smaller



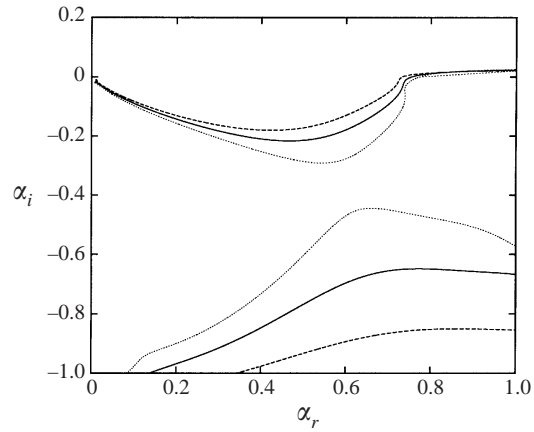


FIGURE 8. Evolution of the spatial branches shown in figure 7 for  $\omega_i = 1.0 \times 10^{-5}$  as the amount of reverse flow is reduced. The dotted line correspond to  $\bar{u}_m = 0.145$  ( $a = -0.25$ ,  $b = 0.92$ ,  $c = 0.216$ ,  $d = 0.22$ ), the continuous line to  $\bar{u}_m = 0.109$  ( $a = -0.25$ ,  $b = 0.92$ ,  $c = 0.20$ ,  $d = 0.19$ ) and the dashed line to  $\bar{u}_m = 0.087$  ( $a = -0.25$ ,  $b = 0.92$ ,  $c = 0.18$ ,  $d = 0.17$ ).

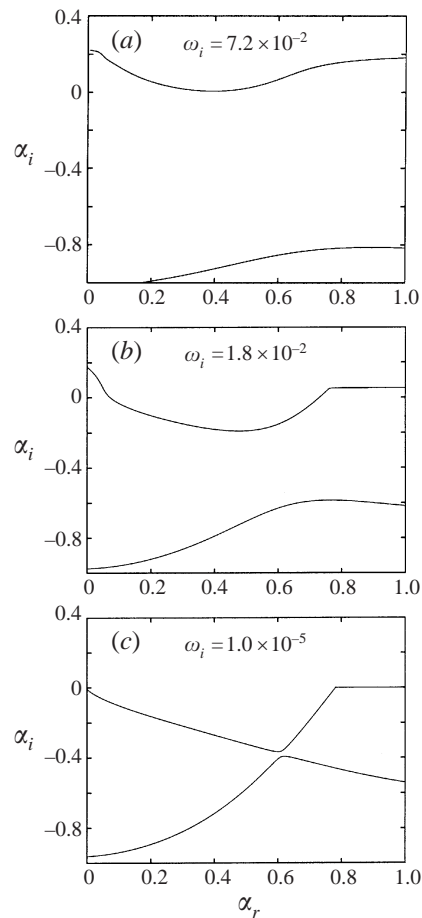


FIGURE 9. Inviscid equivalent of the pinch point in figure 7 for  $\bar{u}_m = 0.145$  ( $a = -0.25$ ,  $b = 0.92$ ,  $c = 0.216$ ,  $d = 0.22$ ) and  $\omega_i = 1.0 \times 10^{-5}$ . This appears to be the minimum amount of reverse flow for the pinch point to occur.

amounts of reverse flow the pinch point occurs at negative  $\omega_i$ , and the instability is then convective in character. It can be concluded that the absolute instability has an inviscid origin and that the existence of reverse flow, although relatively small, is a necessary condition. The same condition was found by Huerre & Monkewitz (1985) for free shear layers ( $\bar{u}_m = 0.136$ ), but this situation may be different in buoyancy plumes and wakes, where the damping and symmetry imposed by the plate are not present, making possible the appearance of absolute instability without reverse flow.

#### 4. Conclusions

In this work we have studied the linear stability characteristics of the mixed convection boundary layer in a uniform stream over a semi-infinite vertical plate at constant temperature. Under these conditions both viscous and buoyancy forces, resulting from the thermally induced density differences, may contribute energy to the growth in time or space of any disturbance present in the flow. Using a coordinate transformation we were able to carry out a continuous analysis from the forced convection regime near the leading edge of the plate, to the free convection regime dominant further downstream. Instead of adopting in advance a pure spatial or temporal instability analysis as in previous studies, the convective or absolute character of the instability was first determined to establish which approach was more appropriate. Taking advantage of accurate numerical methods for the calculation of the basic flow and the solution of the disturbance equations, multiple instability modes coexisting throughout the mixed convection regime have been calculated, thus showing the coexistence of other instability modes in addition to the two previously reported.

When the buoyancy forces are in the same direction as the external flow all the instabilities are convective. For the case of opposing flow, the flow is found to be absolutely unstable beyond a certain threshold of reverse flow. The value of the Reynolds number at which absolute instability first appears increases with diminishing reverse flow, and an inviscid analysis has shown that absolute instability has an inviscid origin.

The analysis in terms of linear convective or absolute instabilities presented here distinguishes open flows that behave as spatial amplifiers from those that show intrinsic dynamics. But in general, as described by Couairon & Chomaz (1996), the transition to global modes due to nonlinear mechanisms will precede the appearance of linear absolute instability, making it a sufficient but not necessary condition for the appearance of global behaviour. This work is intended to provide a more complete linear instability picture of this problem and to be a basis for a subsequent global theory or nonlinear approach, that may uncover new destabilizing mechanisms as well as determine the limits of applicability of the linear analysis.

This research was supported by the Department of Mathematics, Keele University, UK; and P.M. was additionally supported by grant ORS/98020004.

#### REFERENCES

- BERS, A. 1975 Linear waves and instabilities. In *Physique des Plasmas* (ed. C. DeWitt & J. Peyraud), pp. 44–72. Gordon and Breach.
- BETCHOV, R. & CRIMINALE, W. O. 1966 Spatial instability of the inviscid jet and wake. *Phys. Fluids* **9**, 359–362.
- BREVDO, L. 1995 Convectively unstable wave packets in the Blasius boundary layer. *Z. Angew. Math. Mech.* **6**, 423–436.

- BREUDO, L. & BRIDGES, T. J. 1997 Local and global instabilities of spatially developing flows: cautionary examples. *Proc. R. Soc. Lond. A* **453**, 1345–1364.
- BREWSTER, R. A. & GEBHART, B. 1991 Instability and disturbance amplification in a mixed convection boundary layer. *J. Fluid Mech.* **229**, 115–132.
- BRIGGS, R. J. 1964 *Electron-Stream Interaction with Plasmas*. MIT Press.
- CANUTO, C., HUSSAINI, M. Y., QUARTERONIM A. & ZANG, T. A. 1988 *Spectral Methods in Fluid Dynamics*. Springer.
- COUAIRON, A. & CHOMAZ, J. M. 1996 Global instability in fully nonlinear systems. *Phys. Rev. Lett.* **77**, 4015–4018.
- DOVGAL, A. V., KOZLOV, V. & MICHALKE, A. 1994 Laminar boundary layer separation: instability and associated phenomena. *Prog. Aerospace Sci.* **30**, 61–94.
- GASTER, M. 1968 Growth of disturbances in both space and time. *Phys. Fluids* **11**, 723–727.
- HEALEY, J. J. 1995 On the neutral curve of the flat-plate boundary layer: comparison between experiment, Orr-Sommerfeld theory and asymptotic theory. *J. Fluid Mech.* **288**, 59–73.
- HEALEY, J. J. 1998 Characterizing boundary-layer instability at finite Reynolds numbers. *Eur. J. Mech. B Fluids* **17**, 219–237.
- HERBERT, T. 1990 Linear.x A code for linear stability analysis. In *Instability and Transition Vol. II* (ed. M. S. Hussaini & R. G. Voight), pp. 121–144. Springer.
- HIEBER, C. A. & GEBHART, B. 1971 Stability of vertical natural convection boundary layers: some numerical solutions. *J. Fluid Mech.* **48**, 625–646.
- HUERRE, P. & MONKEWITZ, P. A. 1985 Absolute and convective instabilities in free shear layers. *J. Fluid Mech.* **159**, 151–168.
- HUERRE, P. & MONKEWITZ, P. A. 1990 Local and global instabilities in spatially developing flows. *Ann. Rev. Fluid Mech.* **22**, 473–537.
- HUNT, R. & WILKS, G. 1981 Continuous transformation computation of boundary layer equations between similarity regimes. *J. Comput. Phys.* **40**, 478–490.
- KAPLAN, R. E. 1964 The stability of laminar incompressible boundary layer in the presence of compliant boundaries. *Aeroelastic and Structures Research Lab TR 116-1*. MIT.
- KELLER, H. B. & CEBECI, T. 1971 Accurate numerical methods for boundary layer flows. In *Proc. Intl Conf. Numer. Meth. Fluid Dyn. 2nd, Berkeley, CA* (ed. M. Holt). Springer.
- KRIZHEVSKY, L., COHEN, J. & TANNY, J. 1996 Convective and absolute instabilities of a buoyancy-induced flow in a thermally stratified medium. *Phys. Fluids* **8**, 971–977.
- LANDAU, L. & LIFSHITZ, E. M. 1954 *Mechanics of Continuous Media*. Moscow: Fizmatgiz (In Russian).
- LANDAU, L. & LIFSHITZ, E. M. 1959 *Fluid Mechanics*. Pergamon.
- LEE, S. L., CHEN, T. S. & ARMALY, B. F. 1987 Wave instability characteristics for the entire regime of mixed convection flow along vertical flat plates. *Intl J. Heat Mass Transfer* **30**, 1743–1751.
- LINGWOOD, R. J. 1995 Absolute instability of the boundary layer on a rotating disk. *J. Fluid Mech.* **299**, 17–33.
- LINGWOOD, R. J. 1996 An experimental study of absolute instability of the rotating-disk boundary-layer flow. *J. Fluid Mech.* **314**, 373–405.
- MUCOGLU, A. & CHENG, T. S. 1978 Wave instability of mixed convection flow along a vertical flat plate. *Numer. Heat Transfer* **1**, 267–283.
- TAM, C. K. W. 1971 Directional acoustic radiation from a supersonic jet generated by shear layer instability. *J. Fluid Mech.* **46**, 757–768.
- TWISS, Q. 1951 On oscillations in electron streams. *Proc. Phys. Soc. B* **64**, 654–669.
- WOODLEY, B. M. & PEAKE, N. 1997 Global linear stability analysis of thin aerofoil wakes. *J. Fluid Mech.* **339**, 239–260.